Polymer Journal
https://doi.org/10.1038/s41428-022-00662-8

ORIGINAL ARTICLE

A comprehensive study of the structure and piezoelectric response of biodegradable polyhydroxybutyrate-based films for tissue engineering applications

Roman V. Chernozem[1,2] · Igor O. Pariy[1,2] · Artem Pryadko[1,2] · Anton P. Bonartsev[3] · Vera V. Voinova[3] · Vsevolod A. Zhuikov[4] · Tatiana K. Makhina[4] · Garina A. Bonartseva[4] · Konstantin V. Shaitan[3] · Vladimir V. Shvartsman[5] · Doru C. Lupascu[5] · Konstantin N. Romanyuk[6,7] · Andrei L. Kholkin[1,6,7] · Roman A. Surmenev[1,2] · Maria A. Surmeneva[1,2]

Received: 3 February 2022 / Revised: 9 March 2022 / Accepted: 21 April 2022

Abstract

The results of comprehensive research on the thermal behavior and molecular and crystalline structures of poly(3-hydroxybutyrate) (PHB) and poly(3-hydroxybutyrate-co-3-hydroxyvalerate) (PHB-HV) films of different thicknesses, their molecular weights (M_w) and 3-hydroxyvalerate (3-HV) contents are reported. Increasing film thickness from 30 to 100 µm resulted in an isotropic crystal orientation, reducing the crystallite size of the orthorhombic α-phase in the *b* direction from 22 to 17 nm and increasing the degree of crystallinity of the PHB films without affecting their thermal behavior. Furthermore, despite resulting in the same degree of crystallinity and roughness, an ~8-fold decrease in PHB M_w from 803 kDa to 102 kDa resulted in a decreased number of piezoactive domains. The addition of 5.9% 3-HV resulted in anisotropy in the PHB crystalline structure and increased $D_{(020)}$ from 19 nm to 24 nm. Additionally, a further increase in the 3-HV content to 17.5% in the PHB-HV films led to a decrease in the melting temperature and a decrease in the degree of crystallinity from 57% to 23%, which resulted in the absence of local piezoresponse. Notably, the decrease in the M_w of PHB-HV (~17%) from 1177 kDa to 756 kDa resulted in an increase in the degree of crystallinity from 23% to 32%. Moreover, the PHB-HV films became smoother with increasing 3-HV content.

Introduction

Biopolymers are a very promising and important class of materials for regenerative medicine, drug delivery and tissue engineering due to their biocompatibility, diverse physico-mechanical characteristics, and biodegradability [1]. In this regard, polyhydoxyalkanoates (PHAs) have attracted a substantial amount of attention from scientists and engineers. PHAs are natural storage polyesters that are produced by a variety of microorganisms [2].

Among PHAs, poly(3-hydroxybutyrate) (PHB) and its copolymers are likely to be the most well-known and widely

Supplementary information The online version contains supplementary material available at https://doi.org/10.1038/s41428-022-00662-8.

✉ Maria A. Surmeneva
surmenevamaria@mail.ru

[1] Piezo- and Magnetoelectric Materials Research & Development Centre, Research School of Chemistry & Applied Biomedical Sciences, National Research Tomsk Polytechnic University, 634050 Tomsk, Russia

[2] Physical Materials Science and Composite Materials Centre, Research School of Chemistry & Applied Biomedical Sciences, National Research Tomsk Polytechnic University, 634050 Tomsk, Russia

[3] Faculty of Biology, M.V. Lomonosov Moscow State University, 119234 Moscow, Russia

[4] Research Centre of Biotechnology of the Russian Academy of Science, 119071 Moscow, Russia

[5] Institute for Materials Science and Center for Nanointegration Duisburg-Essen (CENIDE), University of Duisburg-Essen, 45141 Essen, Germany

[6] Department of Physics & CICECO−Aveiro Institute of Materials, University of Aveiro, 3810-193 Aveiro, Portugal

[7] School of Natural Sciences and Mathematics, Ural Federal University, Ekaterinburg, Russia

Published online: 14 June 2022

used biocompatible polymers, particularly in tissue engineering, due to their versatility, combination of favorable mechanical properties, minimal tissue toxicity and biodegradability [3–5]. In addition, PHB has a constant local pH during degradation, which makes PHB highly compatible with cells and immune systems [6]. This feature distinguishes PHB from other clinically used polymers, such as poly(lactide glycolide) (PLGA), poly(ε-caprolactone) (PCL), poly (glycolic acid) (PGA), and poly(lactic acid) (PLA) [7]. A controlled biosynthesis of PHB by producer strain *Azotobacter chroococcum 7B* has been reported, and this technology makes it possible to obtain PHB and PHB-HV copolymers with desired monomer compositions, molecular weights and biodegradation rates [8].

Along with its biodegradability and biocompatibility in vitro and in vivo, PHB exhibits piezoelectric properties [9–11], which play a key role in healing [12] and recovery of the heart [13], bone, and nerve tissues [14, 15]. The piezoelectric effect refers to the ability of a material to generate electric charges in response to mechanical deformation caused by an external force [16]. The electric charges generated by the piezoelectric effect cause a cellular reaction, especially in cells that belong to electrically excitable tissues [17]. Moreover, the authors of study [11] showed that the porosity and piezoresponse affect the deposition of $CaCO_3$ under dynamic mechanical conditions, which leads to a more uniform distribution of $CaCO_3$ over the entire PHB scaffold volume. In addition, piezoelectricity can result in the inhibition of biofilm formation [18, 19]. Therefore, PHB is exceptionally promising in the field of biomedicine, for example, for the replacement and healing of cartilage, cardiovascular tissue, skin, bone marrow, and nerve conductors.

However, a relatively high crystallinity, rigidity and low elongation at break can limit bioapplications of homopolymer PHB [20]. Incorporation of 3-hydroxyvalerate (3-HV) into the PHB chain leads to an improvement in the mechanical and physicochemical properties of the polymer [21]. The poly(3-hydroxybutyrate-co-3-hydroxyvalerate) (PHB-HV) copolymer is a potential candidate for tissue engineering and drug delivery purposes due to its biocompatibility, biodegradability, and nontoxicity [14, 22–24]. An increase in the HV content leads to a decrease in crystallinity, thereby resulting in greater flexibility, strength, and elongation at break and resulting in a higher degradation rate [25]. Moreover, the melting temperature of PHB-HV decreases with increasing 3-HV content from 178 °C for pure PHB to 108 °C for P(HB-co-95%HV). PHB-HV with HV contents below 37 mol.% possesses a PHB crystal structure, while PHB-HV with compositions varying from 53 to 95 mol.% 3-HV crystallizes according to the P(3HV) lattice [26]. These changes in the molecular structure and degree of crystallinity result in a significantly lower piezoelectric response for PHB-HV compared with pure PHB, thereby leading to a significantly lower amount of the bioactive ceramics deposited as bone filling for $CaCO_3$ under dynamic mechanical conditions [11]. Thus, the structure of biopolymers determines their successful usage in tissue engineering.

Depending on the intended biomedical applications of the PHB and PHB-HV biopolymers, certain properties are required. Apart from the HV content, their molecular weight and thickness also influence their structure and thereby the properties of the PHB and PHB-HV biopolymer products. The physical limitation of sample thickness affects properties such as molecular chain mobility [27], crystal growth rate [28], and crystallinity [29]. The authors of study [30] demonstrated that decreasing the molecular weight by more than 400 times results in a reduction in PHB crystallinity and an improvement in the mechanical performance without doping with 3-HV. Notably, the crystalline structure affects the mechanical properties, biodegradation kinetics, and biocompatibility of PHB and its copolymers, as reported elsewhere [8, 31]. Moreover, it was demonstrated that changes in the crystalline structure of PHB scaffolds significantly influence their piezoresponse [32, 33]. In turn, the piezoresponse of materials allows the electrical stimulation of cells [17]. In addition, the rate of drug release can be controlled by changing the molecular weight of PHB [34]. These previous studies have focused on the development of new PHB-based blends by mixing PHB with other PHAs, cellulose, polysaccharides, etc. [20]. However, the effects of thickness, molecular weight, and HV content on the structure and properties of PHB and PHB-HV have not been studied in detail thus far.

Thus, the present work aims to investigate the influence of molecular weight, thickness and 3-HV content on the thermal behavior, degree of crystallinity and the crystalline and molecular structures of PHB and its PHB-HV copolymer.

Materials and methods

Materials

The sodium salt of valeric (pentanoic) acid (VA) and the components of the growth medium (K_2HPO_4 $3H_2O$, $MgSO_4$ 7 H_2O, NaCl, Na_2MoO_4 $2H_2O$, $CaCO_3$, $FeSO_4$ 7 H_2O, sodium citrate, $CaCl_2$, KH_2PO_4, sucrose, agar, phosphate buffer saline (PBS), chloroform) were purchased from Merck (Germany) and used as received.

Polymer biosynthesis

The strain *A. chroococcum* 7B was used to produce PHB and its copolymers PHB-HV. Previously, *A. chroococcum*

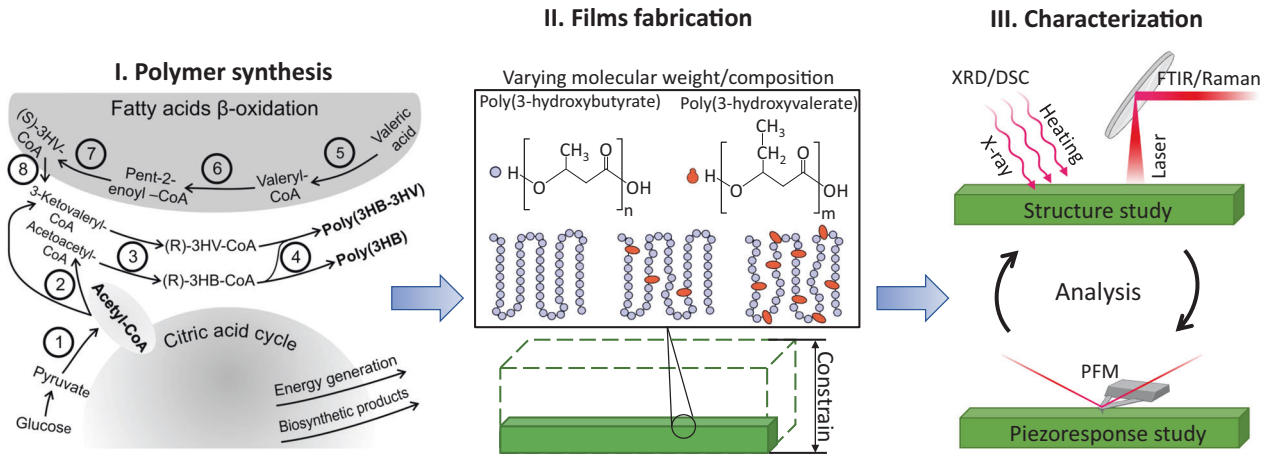

Fig. 1 Schematic illustration of the procedures used in the present study, including polymer synthesis with the subsequent fabrication of films of various thicknesses, molecular structures (PHB or PHB-HV) and weights as well as further film characterization

7B was demonstrated to accumulate PHB to a level of up to 85% of its dry cell weight [35]. The strain was maintained on Ashby's medium. To produce PHB, *A. chroococcum* 7B was grown in shaker flasks with 100 mL of Burk's medium at 30 °C at 250 rpm using an Innova 43 (New Brunswick Scientific, USA)-incubated shaker. Sucrose was used in Burk's medium as the main carbon source. For PHB copolymer biosynthesis, additional carbon sources were added to Burk's medium: 5, 10, 20, 35, and 150 mM valeric acid sodium salt (VA) were added after 0, 4, 12, and 18 h of strain cultivation as a 3-HV precursor in the PHB–HV copolymer chain. The biomass yield and the polymer yield were evaluated as the main parameters for PHB and PHB-HV biosynthesis. Then, PHB and PHB-HV were isolated and purified from the *A. chroococcum* biomass by successive polymer extractions from the biomass with chloroform, polymer precipitation with isopropyl alcohol, filtration, and drying [35].

The proton (^{1}H) NMR spectra of the deuterated chloroform solutions of the purified PHB and PHB-HV were recorded using an MSL-300 (Bruker, Germany) spectrometer at a working frequency of 400 MHz. The molar percentage of 3-HV residues in the PHB–HV copolymer was calculated as the ratio of the integrated signal intensity from the 3-HV methyl groups (0.89 ppm) to the sum of the integrated signal intensities from the methyl groups of 3-HV and 3-hydroxybutyrate (1.27 ppm). Viscosimetry (RT RheoTec viscometer, RheoTec, Germany) was used to determine the molecular weight of the produced polymers (Supplementary Materials, Table S1). Previously, data obtained by viscosimetry (M_w^V) were correlated with data obtained by gel permeation chromatography (GPC) according to a method by Bonartsev et al. [35].

Polymer film fabrication

The biosynthesized polymers were used for the fabrication of films with a variety of thicknesses, molecular compositions (PHB or PHB-HV), and weights for further characterization (Fig. 1), which is described in the next section.

A series of films with thicknesses in the range of 30–100 μm and diameters of 90 mm were cast from the PHB and PHB-HV solutions (Table 1). As a first step, polymers (250–800 mg) were dissolved in chloroform (20–70 mL) overnight at room temperature. Subsequently, polymer films were prepared by casting using degreased Petri dishes. To provide a smooth and uniform film surface, the Petri dishes were held in a perfectly horizontal position and covered with a glass funnel to ensure slow chloroform evaporation. The fabricated films were dried for at least 72 h at room temperature until the solvent had completely evaporated. Then, the polymer films were cut into pieces with dimensions of 30 ± 10 mm^2 [8].

Film characterization

The molecular structure of the thin polymer films was studied by infrared spectroscopy and Raman spectroscopy. Raman spectra were recorded in a range from 110 to 2300 cm^{-1} using a Renishaw InVia microscope with a 50x objective and a 532 nm laser with a maximum power of 100 mW. In addition, 128 spectra for each film were collected using a Tensor 27 Fourier transform IR spectrometer (Bruker, Germany) at a 4 cm^{-1} resolution operating in attenuated total reflection (ATR) mode.

The crystalline structure of the fabricated thin polymer films was evaluated by means of X-ray diffraction (XRD) using an XRD-6000 Shimadzu (Japan) diffractometer with CuKα radiation ($\lambda = 0.154$ nm). XRD patterns were

Table 1 List of fabricated PHB and PHB-HV films with different thicknesses, $M_w{}^V$ and 3-HV contents

Polymer films	Thickness, μm	$M_w{}^V$ kDa	3-HV contents, %
PHB−1 (30)	30	102	0
PHB-1 (60)	60	102	0
PHB-1 (100)	100	102	0
PHB-2	50	803	0
PHB-6 HV	50	794	5.9
PHB-9 HV	50	786	9.1
PHB-17 HV	50	756	16.8
PHB−18 HV	50	1177	17.5

recorded in a 2θ range from 10° to 90° with a step size of 0.01°/2θ at 40 kV and 30 mA. The PDF4+ database was used to analyze the obtained XRD patterns. The crystallite size for the selected Bragg reflections in the fabricated PHB-rGO scaffolds was estimated using the Scherrer Eq. (1):

$$D = \frac{k \cdot \lambda}{\beta \cdot cos\theta} \quad (1)$$

where k is a shape factor; λ is the X-ray wavelength; β is the full width at half maximum intensity; and θ is the Bragg angle.

Differential scanning calorimetry (DSC) of the fabricated polymer films was carried out by a DSC Q2000 instrument (TA instruments) under a nitrogen flux of 20 ml/min in a temperature range of 25 to 250 °C at a heating rate of 10 °C/min. Prior to DSC, the polymer films were hermetically sealed in aluminum pans. The degree of crystallinity of the fabricated scaffolds was calculated using Eq. (2):

$$Xc = \frac{\Delta H_m}{\Delta H_m^0} \times 100\% \quad (2)$$

where ΔH_m is the heat of fusion (J/g) and ΔH_m^0 is the heat of fusion of a 100% crystalline PHB, which equals 146 J/g [36].

The mechanical properties of the films were studied using the nanoindentation method in accordance with ISO 14577. Measurements were carried out using a NanoScan-4D scanning nanohardness tester (TISNCM, Troitsk, Moscow, Russia). Nanoindentation was performed on the smooth side of the films. Films with dimensions of 2×2 mm^2 were fixed with phenyl salicylate. The load was carried out in linear mode; the peak load on the sample was 5 mN. The load time was equal to the unloading time and was 30 s. The peak load was maintained for 5 s. The average penetration depth into the sample was not more than 10% of the film thickness. The mechanical properties were averaged over 6 measurements [8].

The topography and piezoresponse of the PHB and PHB-HV films were evaluated using piezoelectric force microscopy (PFM). PFM measurements were carried out using an MFP-3D atomic force microscope (Asylum Research, USA) equipped with a conductive diamond-coated cantilever DDESP-FM-V2 (Bruker, Germany) with a spring constant of 6 N/m and resonance frequency of 105 kHz. PFM images were acquired from an 8×8 μm^2 surface with a resolution of 256×256 points at a scan rate of 0.1 Hz with a probing *AC* voltage with an amplitude of 8−10 V and a frequency of 500 kHz.

Results and discussion

Effect of film thickness on the PHB structure

The molecular structure of the PHB polymer films of different thicknesses are studied using Raman spectroscopy (Fig. 2A). Independent of the film thickness, all the characteristic peaks assigned to PHB are observed [37], thereby suggesting the absence of an effect of film thickness changes on the molecular composition of the polymer. Moreover, peaks, such as C=O (1725 cm^{-1}), CH_3 (953 cm^{-1}) and C-CH_3 (598 cm^{-1}), corresponding to the crystalline phase, are detected [37–39]. Additionally, XRD analysis reveals Bragg reflections in the PHB films assigned to the orthorhombic α-phase (PDF4 + №00-068-1411) and shows one reflection at ~20° corresponding to the trigonal β-phase (Fig. 2B) [40].

Moreover, XRD analysis demonstrates an influence of thickness on the crystalline structure of the PHB films. As seen from the normalized XRD patterns (Fig. 2B), PHB films with a thickness of 30 μm clearly demonstrate a dominant Bragg peak corresponding to the *(020)* reflection of the orthorhombic α-phase, resulting in anisotropic crystal growth along the *b* direction [41]. In contrast, increasing the film thickness to 60 μm and 100 μm lead to an increase in the intensity of the other Bragg reflections, e.g., at 15–17°, 20–25° and 30–33°, which can be caused by the isotropic orientation of the PHB crystals in thicker films [42]. In addition, the crystallite size in the *b* direction, estimated using Scherrer's Eq. (1) from the *(020)* reflection, decreases from 22 nm to 19 nm and 17 nm with an increase in the PHB film thickness from 30 μm to 60 μm and 100 μm, respectively. The evaluation of the crystallite size in the other directions is a complicated task due to overlapping reflections [41], e.g., *(011)* and *(110)* and *(031)* and *(130)*.

FTIR spectroscopy also demonstrates the presence of the C=O peak (at 1720 cm^{-1}) corresponding to the crystalline structure of the PHB polymer (Fig. 3A) [38, 43]. However, compared with the 30 μm thick films, analysis of the FTIR spectra of the PHB films of thicknesses 60 and 100 μm

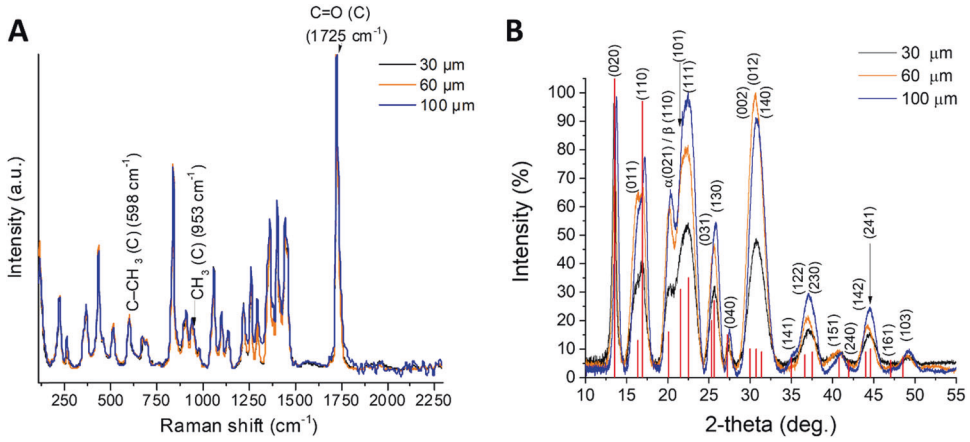

Fig. 2 **A** Raman spectra and (**B**) XRD patterns of PHB films of thicknesses of 30, 60 and 100 μm: C – crystalline phase

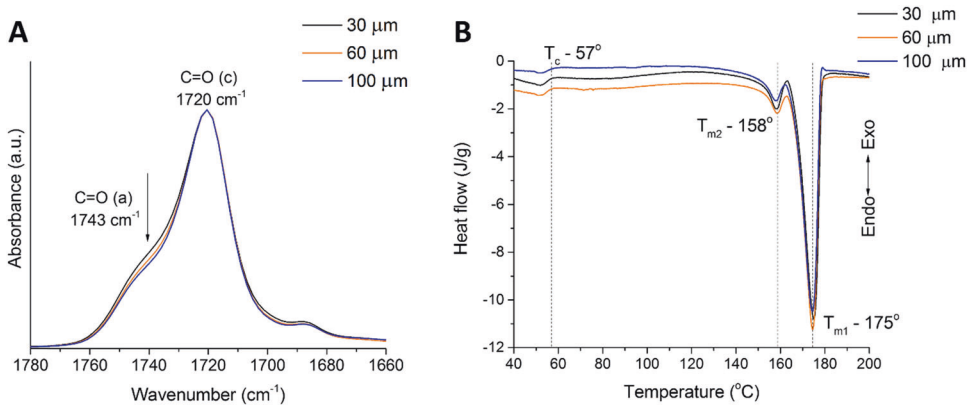

Fig. 3 **A** FTIR spectra in the range of 1780–1660 cm^{-1} and (**B**) DSC curves of PHB films with thicknesses of 30, 60 and 100 μm

shows in a decrease in the intensity of a shoulder to the C=O peak at 1743 cm^1, which is assigned to the amorphous PHB phase [38, 43]. Therefore, the results of FTIR spectroscopy suggest that there are relative changes in the crystallinity of PHB films with increasing thickness.

Furthermore, DSC analysis confirm the results of FTIR spectroscopy (Fig. 3B), i.e., changes occur in PHB film crystallinity with increasing thickness. The calculated degree of PHB film crystallinity (X_c) using Eq. (2) from the DSC curves demonstrate an increase in X_c from 55% to 57% and 61% with increasing film thickness from 30 μm to 60 μm and 100 μm, respectively. Notably, the authors of study [29] also observed an increase in crystallinity with increasing polymer film thickness. In contrast, no influence of film thickness on the PHB thermal properties, such as cold crystallization and melting temperature, is detected. The coexistence of multiple melting peaks for polyesters such as PHB has been widely presented in the literature and has been explained as follows: (i) a simultaneous melting-recrystallization-remelting process [30, 44]; (ii) different degrees of crystallite perfection [44, 45]; and (iii) the presence of several crystalline phases [44, 45].

Thus, a decrease in the PHB microfilm thickness does not affect their thermal properties and molecular composition; however, a decrease in thickness leads to a reduction in the degree of crystallinity of the film and the formation of a more anisotropic crystal PHB structure. Such a relative reduction in the degree of crystallinity is explained by the limited mobility of the polymer chains due to dimensional confinement (film size, e.g., thickness) [46, 47]. Numerous studies have shown similar decreases in crystallinity and confirmed that the crystalline region becomes more anisotropic when the thickness of polymer films decreases [47–49].

Impact of molecular weight on the structure of PHB films

In addition to film thickness, molecular weight can also affect the structure of a polymer, thereby resulting in changes in PHB properties. Therefore, the thermal behavior, crystallinity, and molecular and crystalline structures of PHB films of similar thicknesses with an ~8-fold difference in polymer molecular weight are analyzed.

As in the case of the PHB films of different thicknesses, Raman spectroscopy displays typical peaks for PHB films with molecular weights of 102 kDa (PHB-1) and 803 kDa (PHB-2) (Fig. 4A) [37]. Additionally, peaks for the

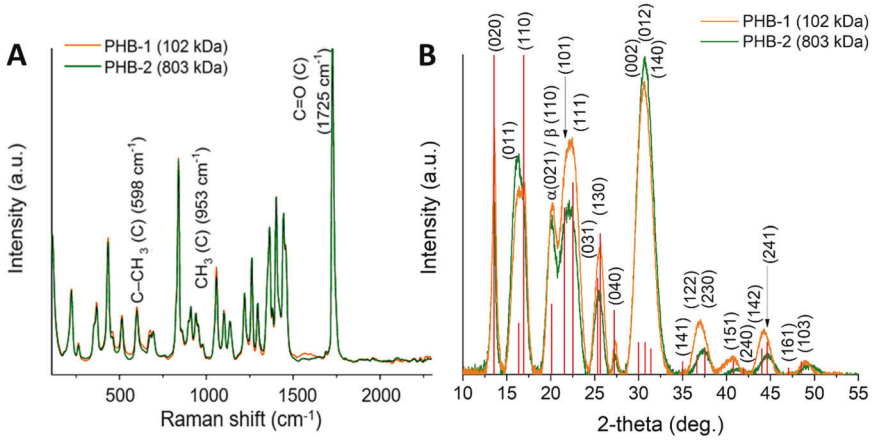

Fig. 4 **A** Raman spectra and (**B**) XRD patterns of the PHB films with M_w values of 102 and 803 kDa

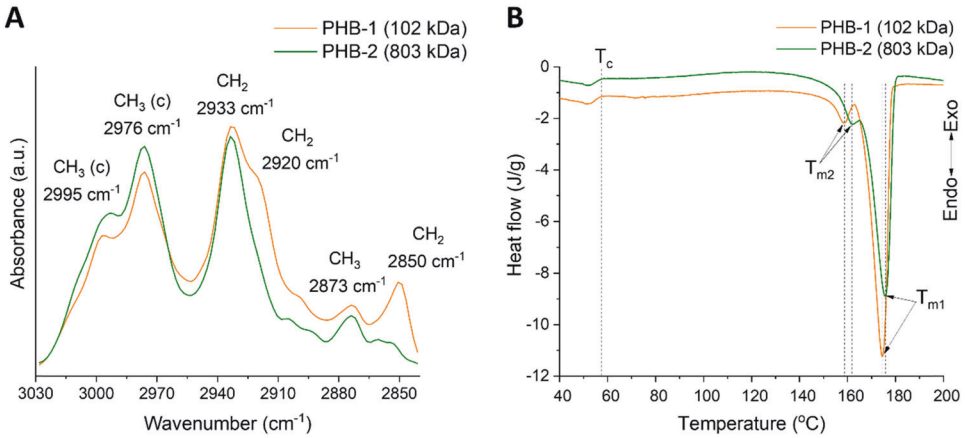

Fig. 5 **A** FTIR spectra in the range of 3030–2835 cm^{-1} and (**B**) DSC curves of the films based on PHB with different M_w values: 102 and 803 kDa

crystalline PHB phase are observed at 598 (C-CH_3), 953 (CH_3) and 1725 cm^{-1} (C=O) [37–39]. XRD analysis also reveals the presence of the orthorhombic α-phase (PDF4 + №00-068-1411) and trigonal β-phase in the PHB films with an ~8-fold differences in molecular weight (Fig. 4B) [40]. The coexistence of several intense Bragg reflections suggests an isotropic orientation of the crystals in the PHB-based films with M_w values of 102 kDa and 803 kDa. An average crystallite size $D_{(020)}$ of 19 nm is obtained for both the 102 kDa and 803 kDa PHB films. However, changes in the intensity of the 15–18° ((110) and (011) reflections) and 22.5–25° ((101) and (111) reflections) regions of the PHB α-phase are detected, which indicates possible changes in the crystal lamellar configurations. By comparing the PHB films of M_w values 750,000 g·mol^{-1} and 1760 g·mol^{-1} (M_w difference >400 times), the authors of study [30] reported larger crystals in PHB films of higher molecular weights.

Figure 5A shows the FTIR spectra in the range of 3030–2835 cm^{-1} for the PHB films with an 8-fold molecular weight difference. Both PHB films demonstrate the absence of a peak at 2987 cm^{-1}, which is assigned to the amorphous phase [50]. However, two new peaks at 2850 and 2920 cm^{-1} are detected in the FTIR spectra of the PHB film of smaller M_w. This difference can be explained by the increased degree of crystallinity [43] or by changes in the molecular structure, since the intensity of the CH_3 peaks of the crystalline phase decrease with a reduction in M_w.

Figure 5B shows the DSC curves of the PHB films of molecular weights of 103 kDa and 803 kDa. In comparison with a reduction in thickness, a decrease in PHB molecular weight leads to opposite changes in the thermal behavior and crystallinity of the films, as shown above (Effect of film thickness on the PHB structure). The cold crystallization temperature (T_c) and X_c of the films are similar and independent of the 8-fold reduction in the PHB molecular weight (Table 2). In this study, an ~8-fold difference in the PHB film M_w is tested, but a greater reduction in the M_w of PHB can result in a decrease in film crystallinity. Significantly reduced crystallinity has been reported in the literature for PHB films of a greater than 400-fold M_w difference [30].

The melting temperature of the films decreases with decreasing PHB molecular weight (Table 2). This change in the melting temperature can be explained by the difference in the size and perfection of the crystals for the films made with different M_w PHB [30, 44]. Moreover, since the same

fabrication conditions were used for all the films, the melting behavior reflects their internal physical structure, which depends on the polymer molecular structure [44, 51]. In addition, a difference is also observed in the Bragg reflections of the PHB α-phase, as mentioned above in the XRD analysis.

The addition of 3-HV to PHB

Figure 6A shows the Raman spectra of the PHB and PHB-HV films containing different 3-HV contents. The PHB films demonstrate the highest 220 cm^{-1} peak intensity (inset, Fig. 5F), while the lowest intensity is observed for the sample with the highest 3-HV content of 17.5% (PHB-18HV). Since low-frequency vibrational motions originate from intramolecular modes strongly associated with intermolecular motions [52, 53], the spectral differences between the samples with low and high 3-HV contents are hypothesized to be the result of differences in the crystalline structures under the influence of intermolecular interactions between the copolymer chains. The crystal structure of PHB has an intermolecular $CH_3 \cdots O{=}C$ hydrogen bond between the C=O group of one helix and the CH_3 group of another helix. In contrast, the crystal structure of PHB-HV has a $CH_2 \cdots O{=}C$ hydrogen bond between the C=O group of one helix and the CH_2 groups of the main chain and side chain [43]. FTIR spectroscopy confirms the presence of the crystalline structure of PHB upon the addition of 3-HV (Fig. 6B). Compared with results for the increase in PHB film thickness, the increase in the 3-HV content of the PHB films leads to an opposite effect on the C=O peak. Increasing the 3-HV content causes an increase in the intensity of the C=O peak shoulder at 1743 cm^{-1}, corresponding to the amorphous phase [38, 43]. Therefore, Raman and FTIR spectroscopy suggest a decrease in the degree of crystallinity of the PHB and PHB-HV films with the addition and increase in the 3-HV content.

Figure 7A shows the XRD patterns of the PHB and PHB-HV films with different 3-HV contents. It is worth mentioning that the intensity of almost all the Bragg reflections for the PHB-HV films is lower than that of the pure PHB films. Compared with the PHB films (PHB-2, Fig. 7A), a 5.9% 3-HV leads to a decrease in the intensity of the Bragg reflections and an increase in the *(020)* reflections of the orthorhombic α-phase (PHB-6HV), resulting in anisotropic PHB-HV crystal growth [54]. In addition, the crystallite size in the *b*-direction increases from 19 nm for pure PHB to 24 nm for the 5.9% 3-HV-containing PHB-HV films. The 17.5% 3-HV-containing PHB-HV films also demonstrate a dominant peak for the *(020)* plane (PHB-18HV, Fig. 7A), and the crystallite size in the *b*-direction is greater (21 nm) than that of the pure PHB films (19 nm). Additionally, the 9.1% 3-HV-containing PHB-HV films show a similar XRD pattern to the PHB films with similar intensities for all Bragg reflections observed. Furthermore, the 9.1% 3-HV-containing PHB-HV films have the same $D_{(020)}$ value (19 nm) as that of the pure PHB films. The same effect of ~9% 3-HV addition was also observed in a previous study [55].

As mentioned above, the ~8-fold difference in the M_w of PHB did not affect the crystalline structure of the films. The XRD pattern analysis reveals a decrease in the intensity of the *(020)* Bragg reflection when the molecular weight is reduced from 1177 kDa to 756 kDa for the PHB-HV films with 3-HV contents of 17% (PHB-17HV) and 18% (PHB-18HV), respectively (Fig. 7B), thereby resulting in a slight decrease in $D_{(020)}$ from 21 nm to a $D_{(020)}$ value similar to that of the pure PHB films (19 nm). At the same time, this reduction in the M_w of the PHB-HV films leads to increasing intensities in all other peaks, suggesting a more isotropically oriented crystalline structure.

Table 2 DSC data for the films based on PHB with M_w values of 102 and 803 kDa

Polymer films	T_c [°C]	T_{m1} [°C]	T_{m2} [°C]	H_m [J/g]	X_c [%]
PHB-1 (102 kDa)	57	174	158	83.3	57
PHB-2 (803 kDa)	57	176	162	82.8	57

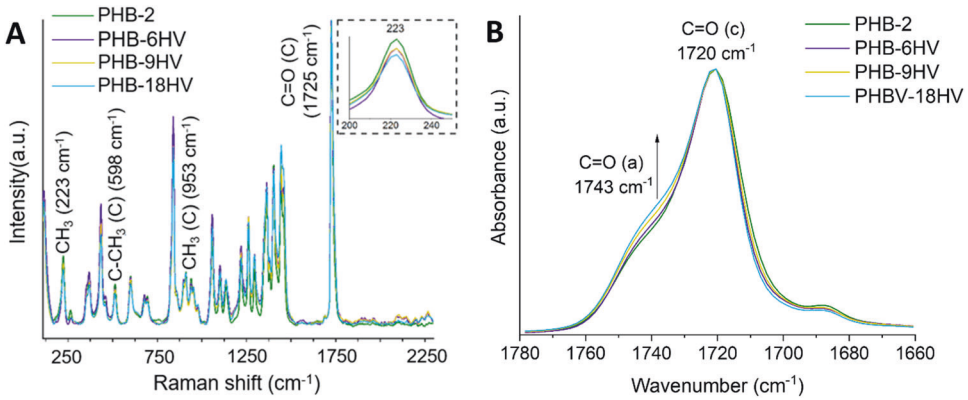

Fig. 6 **A** Raman and (**B**) FTIR spectra in the range of 1780–1660 cm^{-1} for PHB and PHB-HV films with different 3-HV contents

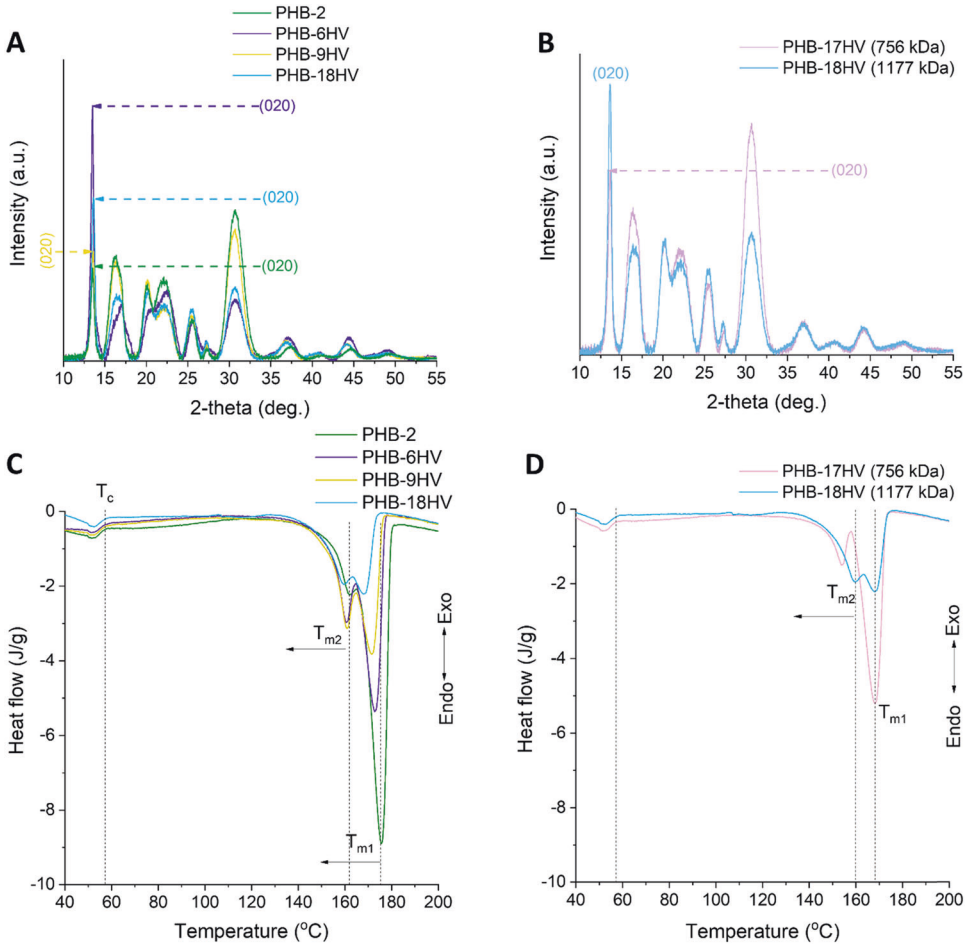

Fig. 7 **A**, **B** XRD patterns of PHB films with different 3-HV contents and PHB-HV films with different molecular weights, respectively. **C**, **D** DSC curves of PHB films with different 3-HV contents and PHB-HV films with different molecular weights, respectively

To characterize the effect of the molecular weight and 3-HV content on the thermal properties and crystallinity of the PHB-HV films, DSC analysis is performed (Fig. 7C, D). Compared with the pure PHB films, no changes in the cold crystallization temperature of the PHB-HV films with increasing HV content are observed (Fig. 7C). Reducing the M_w of the PHB-HV films with 17% and 18% 3-HV does not affect the cold crystallization temperature of the films (Fig. 7D). An increase in the 3-HV added to PHB from 0% to 18% results in a decrease in the melting temperature of the highest peak (T_{m1}) from 176 °C to 168 °C (Table 3). The second melting peak of the PHB-HV film with 18% 3-HV (PHB-17HV, Table 3) demonstrates a lower temperature by 2 °C relative to that of the pure PHB film. Furthermore, a M_w reduction (PHB-HV-7, Table 3) from 1177 kDa to 756 kDa for the PHB-HV films with 17% and 18% 3-HV does not change the temperature (position) of the highest film melting temperature (T_{m1}); however, it reduces the temperature of the second peak (T_{m2}) from 160 to 154 °C. A similar trend is observed for the crystallinity of the PHB and PHB-HV films. Increasing the 3-HV content from 0% to 18% reduces the degree of crystallinity of the PHB films from 5.7% to 23%. A M_w reduction from 1190 kDa to 635 kDa results in an increase in the degree of crystallinity of the PHB-17HV films from 23% to 32% compared with the PHB-18HV films.

Table 3 Cold crystallization and melting temperatures, melting enthalpies and degrees of crystallinity obtained from the DSC results for the PHB and PHB-HV films with different 3-HV contents and different M_w values

Polymer films	T_c [°C]	T_{m1} [°C]	T_{m2} [°C]	H_m [J/g]	X_c [%]
PHB-2	57	175	162	82.8	57
PHB-6 HV	57	173	161	64.4	44
PHB-9 HV	57	172	161	55.0	38
PHB−17 HV	57	168	154	47.2	32
PHB-18 HV	57	168	160	33.7	23

The mechanical properties of PHB and PHB-HV, e.g., Young's modulus, are also studied since these properties are critical for the practical application of medical devices produced from these polymers (Supplementary Materials, Table S2). The data show that the Young's modulus measured by nanoindentation is not dependent on the molecular weight of the PHB homopolymer and decreases almost linearly for the PHB-HV copolymers with an increase in the molar content of 3-HV [8].

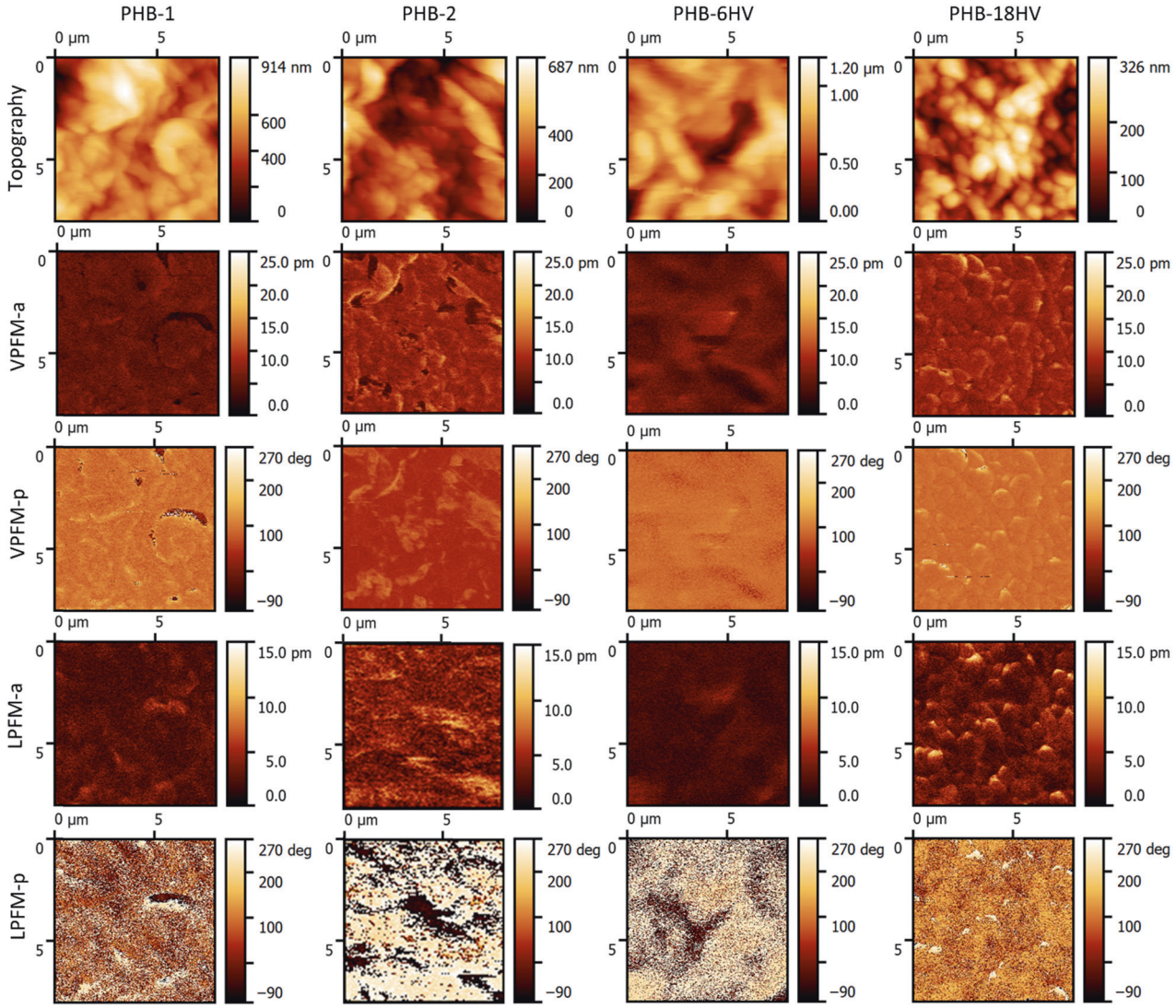

Fig. 8 Topography (first line) and PFM images of vertical (VPFM-a) and lateral (LPFM-a) amplitudes (VPFM-a) and vertical (VPFM-p) and lateral phases (LPFM-p) for PHB films of different molecular weights (~8-fold difference) and 3-HV contents

Topography and piezoresponse of PHB and PHB-HV films

As mentioned above, the variation in the molecular weight or 3-HV content in PHB can have a significant effect on the molecular composition, structure, and degree of crystallinity of the polymer films. In turn, these changes may lead to changes in the topography or piezoresponse of the films. Using advanced techniques, such as scanning probe microscopy, nanoscale insights into the topography and piezoelectric performance of PHB-based films with various molecular weights or 3-HV contents are gained using piezoforce microscopy (PFM), as shown in Fig. 8.

Despite an ~8-fold difference in molecular weight, the PHB films with molecular weights of 102 kDa (PHB-1) and 803 kDa (PHB-2) demonstrate visually similar topographies (Fig. 8). Furthermore, there is no significant difference in the root mean square (RMS) roughness between the PHB-1 and PHB-2 films (Table 4). In contrast, the addition of 3-HV results in changes in the PHB-HV film surface topography. Compared with the other films, the PHB-HV sample with 17.6% 3-HV clearly demonstrates the presence of grain-like features in its topography. Moreover, the RMS roughness is significantly lower in PHBV-18HV, which has the highest 3-HV content (17.6%), compared with the pure PHB films or the PHB-HV films with 5.6% 3-HV (Table 4). This difference in the topography for the PHB and PHB-HV films is explained by the decrease in the degree of crystallinity from 57 % (for PHB-1 and PHB-2) to 23% (for PHB-18HV), as shown in Table 3. A smoother surface was also previously reported for PHB films with a reduction in the degree of crystallinity [47].

Table 4 The root mean square S_q (RMS) roughness of the PHB and PHB-HV films. An (*) asterisk indicates a significant difference ($p < 0.05$)

Films	S_q, nm
PHB−1	119 ± 9
PHB-2	114 ± 3
PHB-6 HV	160 ± 10
PHB−18 HV	63 ± 2*

The analysis of the vertical and lateral PFM signals for the PHB-2 films clearly demonstrates the presence of piezoactive domains (Fig. 8). Despite the same degree of crystallinity in the two films (Table 3), the PHB film with an 8-fold reduction in its molecular weight (PHB-1) exhibits a weaker piezoresponse and fewer piezoactive domains than the PHB-2 film. Taking into account the similar fabrication conditions and the thickness of the PHB-1 and PHB-2 films, we can hypothesize that molecular weight impacts the alignment of molecules, thus affecting the orientation and internal structure of the lamellar crystals and resulting in different piezoresponses. The variation in the length of molecular chains leads to different configurations in the crystalline structure of PHB. For instance, using polarized optical microscopy, the authors of study [30] demonstrated a significant difference in crystal size between PHB films that had a more than 400-fold difference in their molecular weights; however, no differences in XRD patterns were detected for those films. Furthermore, a contrast in the PFM images of polymer films with different lamellar crystal orientations depending on the molecular structure was also shown by Choi et al. [56]. It should be noted that the PHB-1 and PHB-2 films show several differences in their FTIR spectra (Fig. 5A) and XRD patterns (Fig. 4B), such as the presence of CH_2 vibrations (2920 cm^{-1}) and different intensities of the α-phase peak Bragg reflections. In addition, the PHB-1 film demonstrates a slightly reduced melting temperature in comparison with the PHB-2 sample (Table 2), which can be the result of different crystalline configurations. In contrast, the PHB-HV films do not show the presence of piezoactive domains, which can be explained by the significantly reduced degree of crystallinity of the films (Table 3). The observed contrast in the PFM images of the PHB-HV films is strongly correlated with their topography and therefore does not originate from the piezoelectric effect but from electrostatic cross-talk [57]. A decrease in the effective piezoresponse of the PHB-HV films in comparison with PHB films was reported in our previous study [11].

It should also be noted that there are a large number of PHA-producing bacteria, including those existing in the human microbiota [58]. Under natural conditions, the overwhelming majority of these microbes synthesize and accumulate the high-molecular-weight PHB homopolymer. Only some species, such as the bacteria from the genus *Pseudomonas*, synthesize PHB copolymers. Moreover, PHB is used by bacteria not only as a reserve substance but also as a functional molecule used for ion channels and receptors [31, 58, 59]. Thus, taking into account the other unique properties of this natural polymer [31], the piezoelectric properties observed in the high-molecular-weight PHB allow us to assume that the piezoresponse of PHB may have as yet unidentified roles in nature, e.g., serving as a sensor for bacterial communication [59]. Relatively little is known about electrochemical signaling in bacterial communities [60], and this information is of great biomedical significance [18, 19].

Conclusions

In this study, PHB and PHB-HV films of different thicknesses, 3-HV contents and biopolymer molecular weights were fabricated. A decrease in thickness from 100 μm to 30 μm results in similar thermal properties but leads to anisotropic crystal orientation and a slightly reduced degree of crystallinity from 61% to 55% in the PHB films. Moreover, the crystallite size in the *b*-direction for the orthorhombic α-phase of PHB increases from 17 nm to 22 nm with decreasing film thickness from 100 μm to 30 μm. An 8-fold reduction in the PHB molecular weight does not affect the surface roughness or crystallinity; however, it leads to changes in the crystalline structure and thus results in the suppression of piezoactive domains. Additionally, the addition of 3-HV to PHB results in an anisotropic crystal orientation and a decrease in the degree of crystallinity from 57% to 23% with decreasing melting temperature. Compared with the PHB films, a reduction in the PHB-HV molecular weight results in a more isotropic crystal orientation and an increase in the degree of crystallinity from 23% to 32%. Additionally, the PHB-HV films exhibit a smoother surface, with the RMS roughness value significantly decreasing from 119 ± 9 nm (pure PHB) to 63 ± 2 nm (PHB-HV with 17.5% 3-HV). However, the addition of 3-HV to PHB leads to the disappearance of a piezoresponse in the films. Therefore, the thickness, molecular weight and 3-HV content can affect the thermal performance, structure, topography, and piezoresponse of PHB and PHB-HV biopolymer films, and these variations should be taken into account when considering specific biomedical applications for the developed biodegradable thin films.

Acknowledgements This research was performed at Tomsk Polytechnic University within the framework of the Tomsk Polytechnic University Development Program (infrastructure provided for research activities) and was financially supported by the Russian Science Foundation (project number 20-63-47096, sample fabrication and characterization of their properties) and Ministry of Science and Higher Education

(#075-15-2021-588 from 1.06.2021, piezoresponse study). RC, VS and RS acknowledge support from the German-Russian Interdisciplinary Science Center (G-risc) funded by the German Academic Exchange Service (DAAD). This work was developed within the scope of the project CICECO-Aveiro Institute of Materials, UIDB/50011/2020, UIDP/50011/2020 & LA/P/0006/2020, financed by national funds through the FCT/MEC (PIDDAC). We also acknowledge Alexey Rusakov and Alexey Useinov from the Federal State Budgetary Institution "Technological Institute for Superhard and Novel Carbon Materials" for their help in performing previous measurements of the Young's modulus of the PHB and PHB-HV films by nanoindentation.

Compliance with ethical standards

Conflict of interest The authors declare no competing interests.

Publisher's note Springer Nature remains neutral with regard to jurisdictional claims in published maps and institutional affiliations.

References

1. Mohandas SP, Balan L, Gopi J, Anoop B, Mohan PS, Philip R, et al. Biocompatibility of polyhydroxybutyrate-co-hydroxyvalerate films generated from Bacillus cereus MCCB 281 for medical applications. Int J Biol Macromol. 2021;176:244–52.
2. Zhuikov V, Bonartsev A, Bagrov D, Yakovlev S, Myshkina V, Makhina T, et al. Mechanics and surface ultrastructure changes of poly (3-hydroxybutyrate) films during enzymatic degradation in pancreatic lipase solution. Mol Cryst Liq Cryst. 2017;648:236–43.
3. Vieyra H, Juárez E, López UF, Morales AG, Torres M. Cytotoxicity and biocompatibility of biomaterials based in polyhydroxybutyrate reinforced with cellulose nanowhiskers determined in human peripheral leukocytes. Biomed Mater. 2018;13:045011.
4. Shishatskaya EI, Voinova ON, Goreva AV, Mogilnaya OA, Volova TG. Biocompatibility of polyhydroxybutyrate microspheres: in vitro and in vivo evaluation. J Mater Sci Mater Med. 2008;19:2493–502.
5. Altaee N, El-Hiti GA, Fahdil A, Sudesh K, Yousif E. Biodegradation of different formulations of polyhydroxybutyrate films in soil. SpringerPlus. 2016;5:1–12.
6. Meischel M, Eichler J, Martinelli E, Karr U, Weigel J, Schmöller G, et al. Adhesive strength of bone-implant interfaces and in-vivo degradation of PHB composites for load-bearing applications. J Mech Behav Biomed Mater. 2016;53:104–18.
7. Koller M. Biodegradable and biocompatible polyhydroxy-alkanoates (PHA): Auspicious microbial macromolecules for pharmaceutical and therapeutic applications. Molecules. 2018;23:362.
8. Zhuikov VA, Zhuikova YV, Makhina TK, Myshkina VL, Rusakov A, Useinov A, et al. Comparative structure-property characterization of poly (3-Hydroxybutyrate-Co-3-Hydroxyvalerate) s films under hydrolytic and enzymatic degradation: Finding a transition point in 3-hydroxyvalerate content. Polymers. 2020;12:728.
9. Zviagin AS, Chernozem RV, Surmeneva MA, Pyeon M, Frank M, Ludwig T, et al. Enhanced piezoelectric response of hybrid biodegradable 3D poly (3-hydroxybutyrate) scaffolds coated with hydrothermally deposited ZnO for biomedical applications. Eur Polym J. 2019;117:272–9.
10. Chernozem R, Guselnikova O, Surmeneva M, Postnikov P, Abalymov A, Parakhonskiy B, et al. Diazonium chemistry surface treatment of piezoelectric polyhydroxybutyrate scaffolds for enhanced osteoblastic cell growth, Eur. Polym J. 2020;20:100758.
11. Chernozem R, Surmeneva M, Shkarina S, Loza K, Epple M, Ulbricht M, et al. Piezoelectric 3-D fibrous poly (3-hydroxybutyrate)-based scaffolds ultrasound-mineralized with calcium carbonate for bone tissue engineering: inorganic phase formation, osteoblast cell adhesion, and proliferation. ACS Appl Mater Interfaces. 2019;11:19522–33.
12. Castellano D, Sanchis A, Blanes M, Pérez del Caz MD, Ruiz-Saurí A, Piquer-Gil M, et al. Electrospun poly (hydroxybutyrate) scaffolds promote engraftment of human skin equivalents via macrophage M2 polarization and angiogenesis. J Tissue Eng Regen Med. 2018;12:e983–94.
13. Castellano D, Blanes M, Marco B, Cerrada I, Ruiz-Saurí A, Pelacho B, et al. A comparison of electrospun polymers reveals poly (3-hydroxybutyrate) fiber as a superior scaffold for cardiac repair. Stem Cells Dev. 2014;23:1479–90.
14. Gorodzha SN, Muslimov AR, Syromotina DS, Timin AS, Tcvetkov NY, Lepik KV, et al. A comparison study between electrospun polycaprolactone and piezoelectric poly (3-hydroxybutyrate-co-3-hydroxyvalerate) scaffolds for bone tissue engineering. Colloids Surf B. 2017;160:48–59.
15. Young R, Terenghi G, Wiberg M. Poly-3-hydroxybutyrate (PHB): a resorbable conduit for long-gap repair in peripheral nerves. Br J Surg. 2002;55:235–40.
16. Wang AC, Wu C, Pisignano D, Wang ZL, Persano L. Polymer nanogenerators: opportunities and challenges for large-scale applications. J Appl Polym Sci. 2018;135:45674.
17. Huang NF, Lee RJ, Li S. Engineering of aligned skeletal muscle by micropatterning. Am J Transl Res. 2010;2:43.
18. Kumar S, Sharma M, Kumar A, Powar S, Vaish R. Rapid bacterial disinfection using low frequency piezocatalysis effect. J Ind Eng Chem. 2019;77:355–64.
19. Vatlin IS, Chernozem RV, Timin AS, Chernova AP, Plotnikov EV, Mukhortova YR, et al. Bacteriostatic effect of piezoelectric poly-3-hydroxybutyrate and polyvinylidene fluoride polymer films under ultrasound treatment. Polymers. 2020;12:240.
20. Raza ZA, Khalil S, Abid S. Recent progress in development and chemical modification of poly (hydroxybutyrate) based blends for potential medical applications. Int J Biol Macromol. 2020;160:77–100.
21. Steinbüchel A, Debzi E-M, Marchessault RH, Timm A. Synthesis and production of poly (3-hydroxyvaleric acid) homopolyester by Chromobacterium violaceum. Appl Microbiol Biotechnol. 1993;39:443–9.
22. Köse GT, Kenar H, Hasırcı N, Hasırcı V. Macroporous poly (3-hydroxybutyrate-co-3-hydroxyvalerate) matrices for bone tissue engineering. Biomaterials. 2003;24:1949–58.
23. Valappil SP, Misra SK, Boccaccini AR, Roy I. Biomedical applications of polyhydroxyalkanoates, an overview of animal testing and in vivo responses. Expert Rev Med Devices. 2006;3:853–68.
24. Rossi S, Azghani AO, Omri A. Antimicrobial efficacy of a new antibiotic-loaded poly (hydroxybutyric-co-hydroxyvaleric acid) controlled release system. J Antimicrob Chemother. 2004;54:1013–8.
25. Leong YK, Show PL, Ooi CW, Ling TC, Lan JC-W. Current trends in polyhydroxyalkanoates (PHAs) biosynthesis: insights from the recombinant Escherichia coli. J Biotechnol 2014;180:52–65.
26. Kunioka M, Tamaki A, Doi Y. Crystalline and thermal properties of bacterial copolyesters: poly (3-hydroxybutyrate-co-3-hydroxyvalerate) and poly (3-hydroxybutyrate-co-4-hydroxybutyrate). Macromolecules. 1989;22:694–7.
27. Napolitano S, Wübbenhorst M. Deviation from bulk behaviour in the cold crystallization kinetics of ultrathin films of poly (3-hydroxybutyrate). J Phys Condens Matter. 2007;19:205121.
28. Dai X, Li H, Ren Z, Russell TP, Yan S, Sun X. Confinement effects on the crystallization of poly (3-hydroxybutyrate). Macromolecules. 2018;51:5732–41.

29. Frank C, Rao V, Despotopoulou M, Pease R, Hinsberg W, Miller R, et al. Structure in thin and ultrathin spin-cast polymer films. Science. 1996;273:912–5.
30. Hong S-G, Hsu H-W, Ye M-T. Thermal properties and applications of low molecular weight polyhydroxybutyrate. J Therm Anal Calorim. 2013;111:1243–50.
31. Bonartsev A, Bonartseva G, Reshetov I, Kirpichnikov M, Shaitan K. Application of polyhydroxyalkanoates in medicine and the biological activity of natural poly (3-hydroxybutyrate). Acta Naturae. 2019;11:4–16.
32. Chernozem RV, Romanyuk KN, Grubova I, Chernozem PV, Surmeneva MA, Mukhortova YR, et al. Enhanced piezoresponse and surface electric potential of hybrid biodegradable polyhydroxybutyrate scaffolds functionalized with reduced graphene oxide for tissue engineering. Nano Energy. 2021;89:106473.
33. Cai Z, Xiong P, He S, Zhu C. Improved piezoelectric performances of highly orientated poly (β-hydroxybutyrate) electrospun nanofiber membrane scaffold blended with multiwalled carbon nanotubes. Mater Lett. 2019;240:213–6.
34. Bonartsev A, Bonartseva G, Makhina T, Myshkina V, Luchinina E, Livshits V, et al. New poly (3-hydroxybutyrate)-based systems for controlled release of dipyridamole and indomethacin. Appl Biochem Microbiol. 2006;42:625–30.
35. Bonartsev A, Zharkova I, Yakovlev S, Myshkina V, Mahina T, Voinova V, et al. Biosynthesis of poly (3-hydroxybutyrate) copolymers by Azotobacter chroococcum 7B: A precursor feeding strategy. Prep Biochem Biotechnol. 2017;47:173–84.
36. Chen L, Wang M. Production and evaluation of biodegradable composites based on PHB–PHV copolymer. Biomaterials. 2002;23:2631–9.
37. Furukawa T, Sato H, Murakami R, Zhang J, Noda I, Ochiai S, et al. Raman microspectroscopy study of structure, dispersibility, and crystallinity of poly (hydroxybutyrate)/poly (l-lactic acid) blends. Polymer. 2006;47:3132–40.
38. Furukawa T, Sato H, Murakami R, Zhang J, Duan Y-X, Noda I, et al. Structure, dispersibility, and crystallinity of poly (hydroxybutyrate)/poly (L-lactic acid) blends studied by FT-IR microspectroscopy and differential scanning calorimetry. Macromolecules. 2005;38:6445–54.
39. Sato H, Murakami R, Noda I, Ozaki Y. Infrared and Raman spectroscopy and quantum chemistry calculation studies of C–H··· O hydrogen bondings and thermal behavior of biodegradable polyhydroxyalkanoate. J Mol Struct. 2005;744:35–46.
40. Phongtamrug S, Tashiro K. X-ray crystal structure analysis of poly (3-hydroxybutyrate) β-Form and the proposition of a mechanism of the stress-induced α-to-β phase transition. Macromolecules. 2019;52:2995–3009.
41. Liu C, Noda I, Martin DC, Chase DB, Ni C, Rabolt JF. Growth of anisotropic single crystals of a random copolymer, poly [(R)-3-hydroxybutyrate-co-(R)-3-hydroxyhexanoate] driven by cooperative–CH··· O H-bonding. Polymer. 2018;154:111–8.
42. Sun X, Tokuda A, Oji Y, Nakatani T, Tsuji H, Ozaki Y, et al. Effects of molar mass of poly (l-lactide acid) on the crystallization of poly [(R)-3-hydroxybutyrate] in Their Ultrathin Blend Films. Macromolecules. 2012;45:2485–93.
43. Sato H, Ando Y, Dybal JI, Iwata T, Noda I, Ozaki Y. Crystal structures, thermal behaviors, and C− H··· O· C hydrogen bondings of poly (3-hydroxyvalerate) and poly (3-hydroxybutyrate) studied by infrared spectroscopy and X-ray diffraction. Macromolecules. 2008;41:4305–12.
44. Wellen RM, Rabello MS, Fechine GJ, Canedo EL. The melting behaviour of poly (3-hydroxybutyrate) by DSC. Reproducibility study. Polym Test. 2013;32:215–20.
45. Gunaratne L, Shanks R. Melting and thermal history of poly (hydroxybutyrate-co-hydroxyvalerate) using step-scan DSC. Thermochim Acta. 2005;430:183–90.
46. Wang MM, Braun H, Meyer E, Zhu J. Morphogenesis and chain behaviors related to crystallization in ultrathin polymer films. World Sci Tech R D. 2006;28:5–18.
47. Anbukarasu P, Sauvageau D, Elias AL. Enzymatic degradation of dimensionally constrained polyhydroxybutyrate films. Phys Chem Chem Phys. 2017;19:30021–30.
48. Reddy KR, Ogawa S, Sato H, Takahashi I, Ozaki Y. Evolution of intermediate and highly ordered crystalline states under spatial confinement in poly (3-hydroxybutyrate) ultrathin films. Macromolecules. 2016;49:4202–10.
49. Kossack W, Seidlitz A, Thurn-Albrecht T, Kremer F. Interface and confinement induced order and orientation in thin films of poly (ϵ-caprolactone). Macromolecules. 2016;49:3442–51.
50. Sato H, Murakami R, Padermshoke A, Hirose F, Senda K, Noda I, et al. Infrared spectroscopy studies of CH⊙⊙⊙ O hydrogen bondings and thermal behavior of biodegradable poly (hydroxyalkanoate). Macromolecules. 2004;37:7203–13.
51. van Drongelen M, Van Erp T, Peters G. Quantification of non-isothermal, multi-phase crystallization of isotactic polypropylene: The influence of cooling rate and pressure. Polymer. 2012;53:4758–69.
52. Hoshina H, Morisawa Y, Sato H, Minamide H, Noda I, Ozaki Y, et al. Polarization and temperature dependent spectra of poly(3-hydroxyalkanoate)s measured at terahertz frequencies. Phys Chem Chem Phys. 2011;13:9173.
53. Hoshina H, Morisawa Y, Sato H, Kamiya A, Noda I, Ozaki Y, et al. Higher order conformation of poly(3-hydroxyalkanoates) studied by terahertz time-domain spectroscopy. Appl Phys Lett. 2010;96:101904.
54. Owen A, Heinzel J, Škrbić Ž, Divjaković V. Crystallization and melting behaviour of PHB and PHB/HV copolymer. Polymer. 1992;33:1563–7.
55. Sato H, Ando Y, Mitomo H, Ozaki Y. Infrared spectroscopy and X-ray diffraction studies of thermal behavior and lamella structures of poly (3-hydroxybutyrate-co-3-hydroxyvalerate)(P (HB-co-HV)) with PHB-type crystal structure and PHV-type crystal structure. Macromolecules. 2011;44:2829–37.
56. Choi Y-Y, Sharma P, Phatak C, Gosztola DJ, Liu Y, Lee J, et al. Enhancement of local piezoresponse in polymer ferroelectrics via nanoscale control of microstructure. ACS Nano. 2015;9:1809–19.
57. Jesse S, Guo S, Kumar A, Rodriguez B, Proksch R, Kalinin SV. Resolution theory, and static and frequency-dependent cross-talk in piezoresponse force microscopy. Nanotechnology. 2010;21:405703.
58. Bonartsev A, Voinova V, Bonartseva G. Poly (3-hydroxybutyrate) and human microbiota. Appl Biochem Microbiol. 2018;54:547–68.
59. Voinova V, Bonartseva G, Bonartsev A. Effect of poly (3-hydroxyalkanoates) as natural polymers on mesenchymal stem cells. World J Stem Cells. 2019;11:764.
60. Manna SS, Ghanty C, Baindara P, Barik TK, Mandal SM. Electrochemical communication in biofilm of bacterial community. J Basic Microbiol. 2020;60:819–27.